CALIFORNIA INSTITUTE OF TECHNOLOGY

Lindhurst Laboratory of Experimental Geophysics
Seismological Laboratory 252-21, 1200 E. California Blvd.
Pasadena, CA 91125

Thomas J. Ahrens
Fletcher Jones Professor of Geophysics

November 1, 2004

"Impact Processes in the Solar System"

Annual Progress Report

January 1, 2004 to December 31, 2004

NASA/Goddard – Grant NNG04G107G

Thomas J. Ahrens
Principal Investigator

cys: *Stephen Saunders (Technical Officer), orig. hard & electron. copy*
Carolyn Gonser - GSFC (Grant Officer), one copy
ONR (Admin. Grants Officer), letter only
CASI, Attn: Document Processing Section, 7121 Standard Drive, Hanover, MD 21076
(microreproducible copy)

E-MAIL: tja@caltech.edu • TELEPHONE# (626) 395-6906 • FAX# (626) 564-0715, 568-0935
WEB ADDRESS: http://www.gps.caltech.edu/~ahrens

I. OVERVIEW

The three main topics of this program as described initially in our May 2003 proposal are:

1) Shock-induced damage and attenuation in planetary materials.

2) Shock-induced melting and phase changes.

3) Impact-induced volatilization and vapor speciation of planetary materials

Our progress is described in the following sections.

Progress of two other satellite projects (#4 and #5) are not, however, described. Topic 4 has been the subject of a continuing investigation since ~ 1990. On Topic 5, we have a paper in preparation and have submitted a proposal to Astrobiology.

4) Responses of planetary atmospheres to giant impact,

5) Effects of impact-induced shock waves on microbial life

II. RESEARCH TOPICS

1) Shock-induced damage and attenuation in planetary materials.

The goal of this project is to understand the nature of damage zones beneath craters in different planetary materials and relate these to the nature of the impactor and its trajectory. Starting in 1990 with the observation of the different families of cracks from impacts on Earth materials [*Polanskey and Ahrens*, 1990], our program demonstrated that for a range of damage in laboratory and planetary craters, there are two regimes for physical cratering processes (strength and gravity) which also control the distribution of damage. Recently, Ai and Ahrens [2004], demonstrated that damage zones may be described utilizing previous results of shock wave attenuation calculations, and, data for dynamic tensile strength of rocks. These are applied to determine the radius to which significant damage occurs upon impact onto rock targets. Using the Ai and

Ahrens [2004] model, we require either stress wave attenuation data or calculations, as well as a theoretically or experimentally based tensile strength model. In the present program, we are making dynamic tensile strength measurements over a wide range of rock types and expect, in the future, to also study tensile strength and shock damage in low-temperature H_2O ice.

Although hypervelocity impact crater morphology remains virtually circular over a wide range of normal (90°) to oblique 10-15° impact directions, numerical studies indicate that the asymmetric transient shock pressure distribution is expected to be mimicked by the damage (D) distribution.. Here, the angle, θ, is measured with respect to the local horizontal. Although there are a number of field studies of seismic velocity structure beneath impact craters, there has been no previous research on the damage distribution beneath impact craters either in the field or those produced in the laboratory.

To understand damage associated with planetary craters, we have conducted detailed studies on strength – controlled craters in the laboratory. Our present laboratory tools for studying cracked damage beneath craters are ultrasonic velocity and ultrasonic attenuation measurements (in the range of 2-5 MHz). We are performing impacts onto 20 x 20 x 15 cm samples of various rock types, and conducting post-impact seismic sounding of the shock damage within the target rock. Similar to seismic reflection surveys in the field, we use both surface and "drill-hole data" via lateral access to the sides of the impacted sample to define the structure, and as a result, obtain 2- and 3-dimensional compressional wave velocity distributions.

Dynamic loading via impact generates a range of different crack families in minerals and other brittle materials [*Ahrens and Rubin*, 1992]. The impact induced compression and tensional waves in planetary materials produce cracks in brittle media

which result from intense compressional, shear and tensional loading. However, it has long been recognized that although these different loadings take place in rocks, it is only tensional failure that gives rise to cracks and crack damage. Crack damage (D) is taken to vary from 0 to 1.0. For silicates, this corresponds to uncracked material and fully cracked material, respectively.

Dynamic loading via impact generates a range of different crack families in minerals and other brittle media [*Ahrens and Rubin*, 1993]. However, by simplifying and describing cracking as a scaler, a cracked density parameter is defined as

$$\varepsilon \equiv N\langle a^3 \rangle \tag{1}$$

where N is the number of cracks in a unit volume and a is the mean crack length/2.

Crack damage is easily quantified, and hence, related to ε, using ultrasonic measurements of wave propagation velocity and attenuation [*Liu and Ahrens*, 1997]. Damage is related to the fraction of the elastic moduli which is retained. Thus for measurements of the velocity of P- and S-waves (D_p and D_s), damage may be defined as

$$D_p = \left[1 - \left(\frac{V_p}{V_{p0}}\right)^2\right] \tag{2a}$$

$$D_s = \left[1 - \left(\frac{V_s}{V_{s0}}\right)^2\right] \tag{2b}$$

where V_{p0} and V_{s0} are the initial pre-shock elastic velocities and V_p and V_s are elastic velocities of P and S waves in the damaged material. Budiansky and O'Connell [1976] and others have developed a theory for predicting the elastic constant seismic velocity and

attenuation of cracked materials based on damage, which is related to ε via an empirical relation for P-waves [*Liu and Ahrens*, 1997]

$$D_p = 3.4\varepsilon - 1.2\varepsilon^2 \tag{3}$$

For elastic wave propagation, if the amplitude of the elastic wave is decreasing with distance (X) as given by

$$A = A_0 \exp^{(-X\alpha)} \tag{4}$$

the effective (half) crack length in the material which is undergoing attenuation in the stress wave is given by

$$a = \frac{h\varepsilon}{\alpha} \tag{5}$$

where "h" is a material dependent constant.

Later analysis by Ashby and Sammis [1990] developed a theoretical basis for predicting the dependence of the confining quasi static shear strength of deformed rocks. Such constitutive relations are used to describe parameters of planetary surface materials for impact cratering calculations.

In future impact calculations, we expect that we will also be able to take into account the increase in tensile strength with increasing strain rate which can be described in terms of duration, Δt, of tensile wave loading of material such that the tensile strength depends on Δt and is given as

$$\sigma_t = \frac{K_{IC}}{2}\sqrt{\frac{\pi}{V_{OS}\Delta t}} \tag{6}$$

Here, K_{IC} is the stress intensity factor for Mode I tensile fracture (such as the radial cracks going out from impact source) is employed. We have been measuring σt for different values of Δt to determine K_{IC} in spall experiments for a number of unmeasured rock types.

Damage distributions are determined in target rocks from seismic travel times from a series of sources and stations as indicated in Fig. 1a. These yield upon inversion, subsurface structure of the damaged region. During the last year we have investigated the degree to which the resulting inversion is affected by the curvature of seismic rays (resulting from the velocity structure as shown in Fig. 2). Notably, upon taking into account the ray curvature, we found there were only minor differences in the final iterated velocity structure (see Fig. 2b).

Upon internal discussions at Caltech, we realized that our inversions for velocity structure also included a few paths that were within the space of escavated laboratory crater. After editing out these likely erroneous data, we have redone our investigations and we find that the slightly modified structures are obtained by excluding those paths which are not physically realizable as shown in Fig. 3.

Because virtually all laboratory shock impact experiments are in the strength controlled regime, we are attempting to develop numerical methods that faithfully simulate the transition from the strength to gravity regime and provide the basis for extrapolation of damage into planetary-sized craters. Initially, we employed the well known CTH code (Sandia National Laboratories), which employs a failure and rheological model of Johnson-Holmquist (JH) to describe damage via compressional and shear stresses [*Holmquist et al.*, 1993; *Johnson and Holmquist*, 1994]. The J-H model is commonly used for describing impact into light armor ceramics and other engineering

ceramics. On the basis of comparison between the CTH calculations using the JH model and our experiments using granite targets (Fig. 4), we find that these JH models seriously overestimated the zone of intense shock damage. We believe that dynamic properties of granite are sufficiently well known such that uncertainties in properties do not account for this discrepancy. Similarly to Collins et al. [2004], we have concluded from such comparisons, that we need to implement a tensile fracture damage model and expect to start using the Clegg et al. [2002] tensile cracking model for future calculations. The CTH model apparently works well for shear compressional induced cracking in ceramics, but since it doesn't use tensional cracking to describe damage, it is incapable of dealing with the tensile features that dominate rock damage.

The asymmetric damage for oblique impacts appears to be quite a promising way to obtain impactor direction from the orientation and dip of the peak shock damage zone beneath craters. We find, in agreement with the oblique impact calculations published by Pierazzo and Melosh [2000], that the down range direction of impact is the direction where damage from an oblique impact takes place preferentially. However, details of the damage distribution (e.g. relation of angle of impact and dip of the axis of peak subsurface damage) requires further study. We also expect to study the transition of the strength to gravity regime with respect to crater damage, for normal and oblique impact via calculations.

Of special interest is the interaction of the regions of net tension associated with the impact-induced shock with the static, lithostatic compressional stress field. The suppression of tensile cracking, at depth, on account of the overburden compressive stress depends on target density, and impact parameters. The suppression of tensile cracking because of gravity has not yet been studied and is also on our agenda of future effort.

With the goal of constraining impact parameters, we expect to conduct predictive calculations of shock damage beneath large terrestrial impact craters such as the Chicxulub and Chesapeake Craters, and compare these to seismic logging and core-sample velocity data as these become available.

The theory of Budiansky and O'Connell yields the relationship between damage and crack number density. To describe the damage from different materials, we need to also determine the effective crack length. To this end we use Eq. 5 and have started an effort to conduct attenuation measurements in cracked rocks. The more damage the rock suffers, the more attenuative it is, and we find an excellent correlation between the damage and increased attenuation which via a simple theory, provides a good measure of the length of cracks associated with damaged regions.

Damage studies are new and expected to be useful to study planetary impact cratering data and what they tell us about the origin and evolution of planets and life.

2) Shock-Induced Melting and Phase Changes

Heavily shocked chondrite and achondrite meteorites have provided natural, and in some cases, the only natural samples of the high-pressure phases of mantle minerals of the Earth. The high-pressure phases observed in ferromagnesium minerals of shocked meteorites including high-pressure phases of olivine --- wadsleyite, ringwoodite, and the perovskite and magnesio-wüstite assemblage (of the lower mantle). For pyroxenes, high-pressure phases of akimotoite, majorite, and perovskite are found in nature as is stishovite and post-stishovite high pressure phases of SiO_2, in the $CaCl_2$, and α-PbO_2 structures. The latter were discovered in SNC meteorites. Also recovered from shocked meteorites are the high-pressure phases of feldspars transformed to the hollandite structure, and the

CaNa hexa-alumino-silicate structures. In most cases, the high-pressure phases are found on the edges of what appears to be shock-induced melt regions, whereas in some shocked meteorites the high-pressure phases are clearly produced via the solid state. Recent microscopic studies of the textures of the shocked meteorites by Thomas Sharp at Arizona State University, Jean-Paul Poirier, and P. Gillet in Paris, as well as, thermal analysis conducted by P. DeCarli indicate that the high-pressure phases, in some cases form from the melt. In other cases, they showed that a solid-state origin resulted from excessively heating, and also as a result of shock deformation.

Our recent experiments were motivated by the notable lack of success of previous experiments to recover high-pressure phases from plane-wave shock recovery experiments, and the obvious need for local high temperatures, as observed previously, in our oblique sliding experiments [*Potter and Ahrens*, 1994]. We utilize our previous geometry which has been used to synthesize spinel from oxides, as well as conduct consolidations of mineral powders (e.g. Schwarz et al. [1984b] and [1984a], Potter and Ahrens [1987], and Ahrens and Potter [1988]).

Our group has now conducted four experiments patterned after the Potter and Ahrens [1994] results and demonstrated that the shock melting occurs as it did for the MgO-Al_2O_3 formulation. In our sliding experiments, melting occurs at relatively modest shock loading pressures, below those predicted to produce melt in plane geometry. In the cases of MgO-SiO_2 (fused quartz), and Mg_2SiO_4-SiO_2 samples, the melt production of the interface is intermediate in composition. In three experiments, high pressure phases are seen. Wadsleyite and ringwoodite have been recovered, and another what we believe is a not previously described high-pressure phase was identified with micro-Raman, as well as x-ray diffraction using a synchrotron source at Argonne National Laboratory.

Although only a few experiments have so far been conducted, we feel the results are very successful and we are very encouraged to pursue this line of research and expect to put theoretical efforts in to understand the thermodynamics of the sliding phenomenon.

3) Impact-induced Volatilization and Vapor Speciation of Planetary Materials

Upon planetary impact a shock wave is generated in minerals and this gives rise to shock heating which at sufficient intensities causes melting and vaporization to occur. Using the usual shock wave equations of state, Grüneisen parameters of minerals, and specific heats, the shock temperatures and corresponding increases in entropy are calculated. However, upon shocking materials, the details of driving off different species in the vapor depends critically on which species are present in the vapor. These are poorly understood at low temperatures. At elevated temperatures (~10^3 K and greater), the thermodynamic calculations that are conducted for incongruent vaporization are expected to be reliable, as reaction-rate effects are overcome by the high temperatures. What is required then, is the ability to measure the population of all species in gas, especially positive ions, and neutrals for shocks at < 10^3°K. For example, the onset of impact vaporization of water ice and other water related substances [*Tyburczy et al.*, 1990] are presently poorly predicted by straightforward thermodynamic calculations. Impacts in excess of 5 km/s are expected on the basis of thermodynamic properties of ice to be required for vaporization. Sugi et al. [1998] conducted impact experiments in a vacuum chamber that are similar to what we are gearing up to do, but he used a resonance ionization mass spectrometer, and determined that for porous ice, only 2 MPa shock pressure is required for vaporization and ionization and this is achieved with impactors at 100 m/s. Much lower velocities than predicted theoretically are required to produce water

vapor ions in his mass spectrometer. Sugi et al.'s [1998] results suggested that the ordinary thermodynamic calculations are very much in error with regard to shock vaporization. Because of the ice data, and previously noted discrepancies with theory, we expect to wage a major campaign to get speciation data for various ices. We believe these data will be valuable for interpreting the Cassini Cosmic Dust Analyzer results and also the results of the Deep Impact experiment.

Previously, our group has had a long history of studying both impact vaporization, both theoretically and experimentally, starting with the work of Ahrens and O'Keefe [1972], Boslough et al. [1980], and Lange and Ahrens [1982]. In these experiments shock pressure versus mass fraction vaporization was measured, but the vaporized species were not specified or measured. Speciation is of great importance for many impact vaporization issues, for example, in the case of the impact vaporization of gypsum to form SO_2 at the K/T boundary. It has long been believed that depending on the temperature, SO_2 forms at lower temperature than SO, however, SO has a very large cooling effect on the Earth because it slowly oxidizes to SO_2 in the atmosphere, and when SO_2 forms, it immediately combines with ice particles in the ionosphere, to form stratospheric sulfuric acid clouds. These cause global cooling on account of the decreasing sunlight incident on the surface of the Earth. However, if more SO_2 forms, then it is expected that, the global cooling interval after a giant impact is much shorter because there is no time delay in producing all the possible sulfuric acid aerosol from the stratospheric water. The scenario that has been pursued on this by, i.e. Pope et al. [1997], indicates that due to the long time-scale required to oxidize SO to SO_2, a 10 year time span of global cooling occurs. This has a large effect on the environment, and has severe

effects on biota on a global basis, and gives rise to mass extinctions, whereas global cooling of 6-12 months is unlikely to have this effect.

Previously, the techniques of vaporizing samples to study speciation employed laser impact [*Ahrens et al.*, 2003; *Jyoti et al.*, 1999]. Laser impact, unfortunately, only provides loose bounds on the shock state produced. To address the shortcomings of laser impact, we developed a micro-explosive launch flyer plate that operates in vacuums of 10^{-7} torr (Fig. 5). The 0.5 mm thick flyer plate is launched to 1-2 km/s.

Earlier shock wave data for calcite and gypsum have been enhanced by the time-of-flight mass spectra shown in Figs. 6 and 7. We expect to now conduct these experiments using impactors with measured velocities.

We expect to study virtually all the previously studied minerals investigated with the laser technique, and will expect to look at how the speciation varies with time after impact vaporization by using the extraction pulse in the time-of-flight mass spectrometer to extract different portions of the vapor plume out of the system for mass spectroscopy. We expect to also measure, using the electron impact ionization system shown in Fig. 5, the population of neutral and positive ions in the gas. Initial data for water and water-related materials as ices were obtained using the cold finger in the mass spectrometer arrangement shown in Fig. 8. Initial data for H_2O and H_3O are shown in Fig. 9. Typical spectra for water shown in Fig. 9 and Fig. 10 gives a spectra for D_2O.

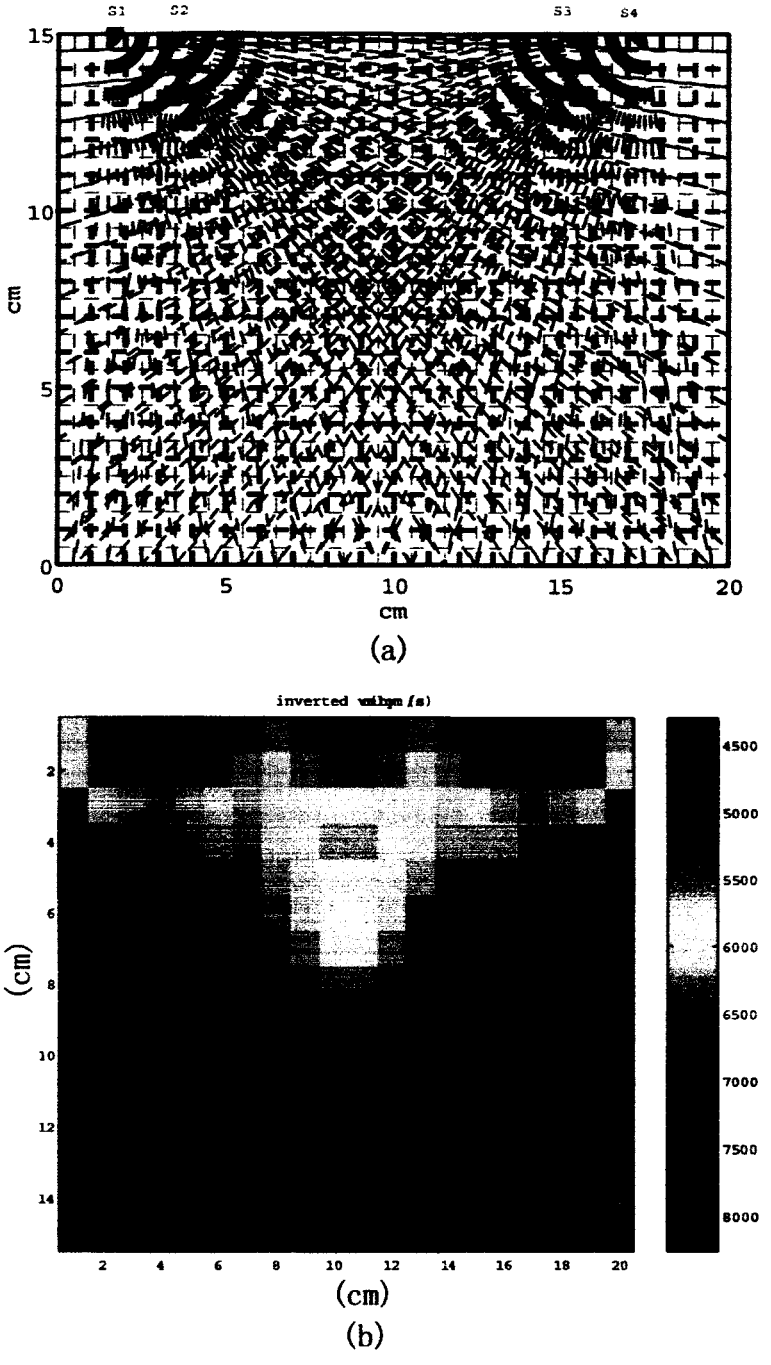

FIGURE 1. (a) Tomographic straight ray diagram. Thick dashed lines are the cell boundary and thin dashed lines are the ray distribution. Four pneumatic impactor sources (S1-4) are used for this survey, and receiver stations, employing 5 x 5 mm, PZT P-wave transducers, with 1 cm increment, were placed on two other surfaces. A 0.05 cm thick buffer tungsten carbide plate is placed at the impact point to prevent producing micro-craters; (b) Smoothed compressional wave velocity structure of the post-shot target assuming straight ray paths. The cracked low velocity zone extends to depth of ~ 7 cm for this shot.

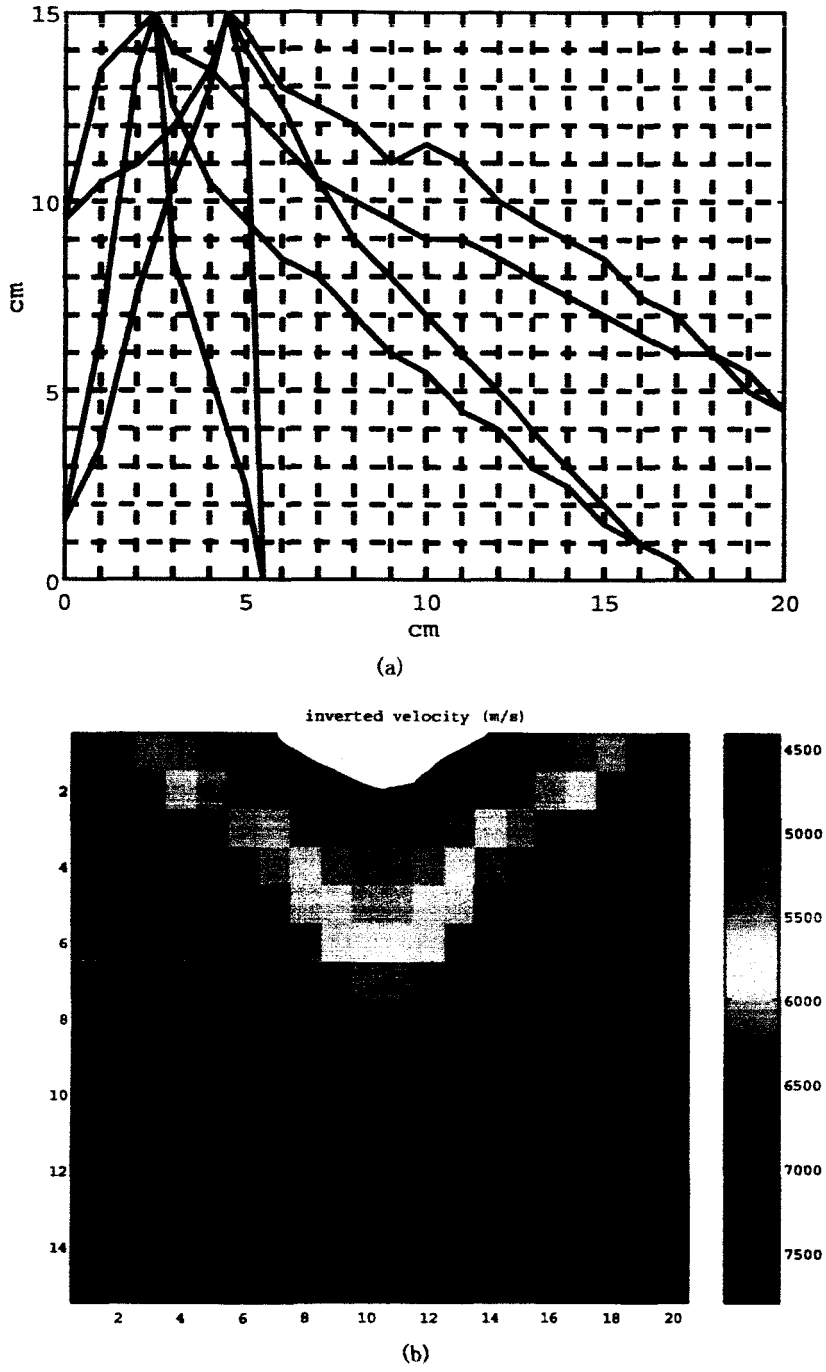

FIGURE 2: (a) Tomographic diagram showing a few curve ray examples dependent on the velocity model; (b) Smoothed compressional wave velocity structure of the center plane for the first iteration assuming curve ray path. The low velocity zone extends to ~7 cm as no obvious improvement over the straight ray assumption inversion result (of FIGURE 1b) iteration was stopped.

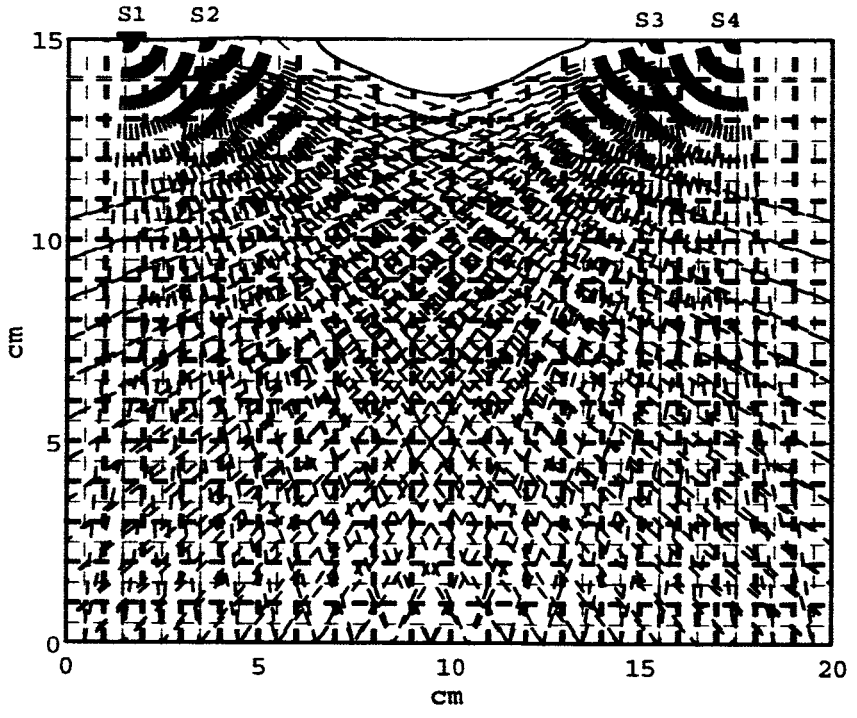

(a)

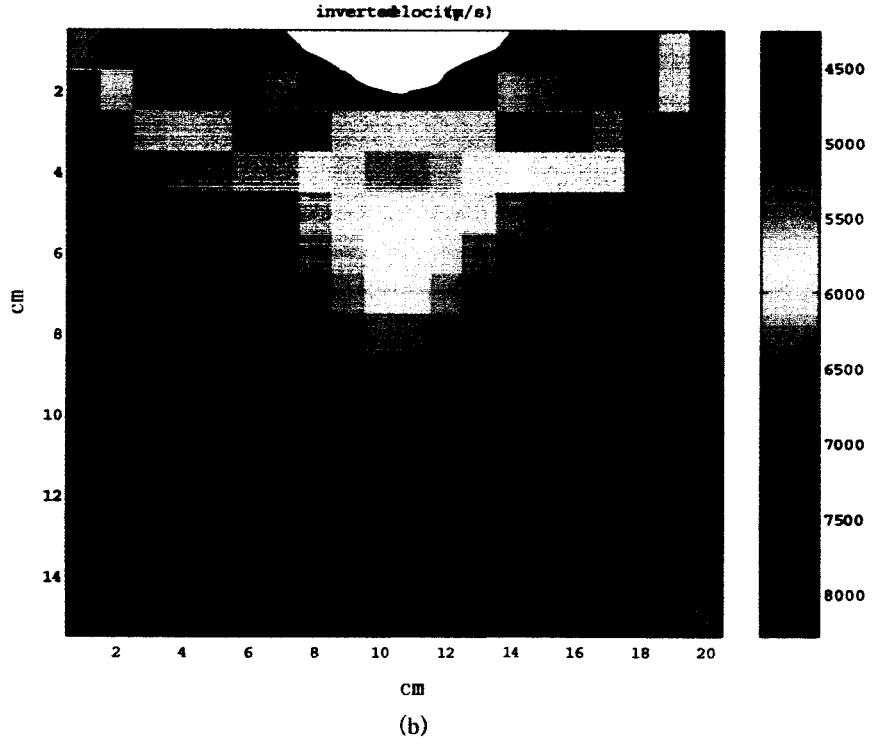

(b)

FIGURE 3: (a) Tomographic straight ray diagram similar to FIGURE 1a, except that those rays crossing the excavated crater are taken out. (b) Smoothed compressional velocity structure using only the rays not crossing the excavated crater. The excavated crater is shown in both figures.

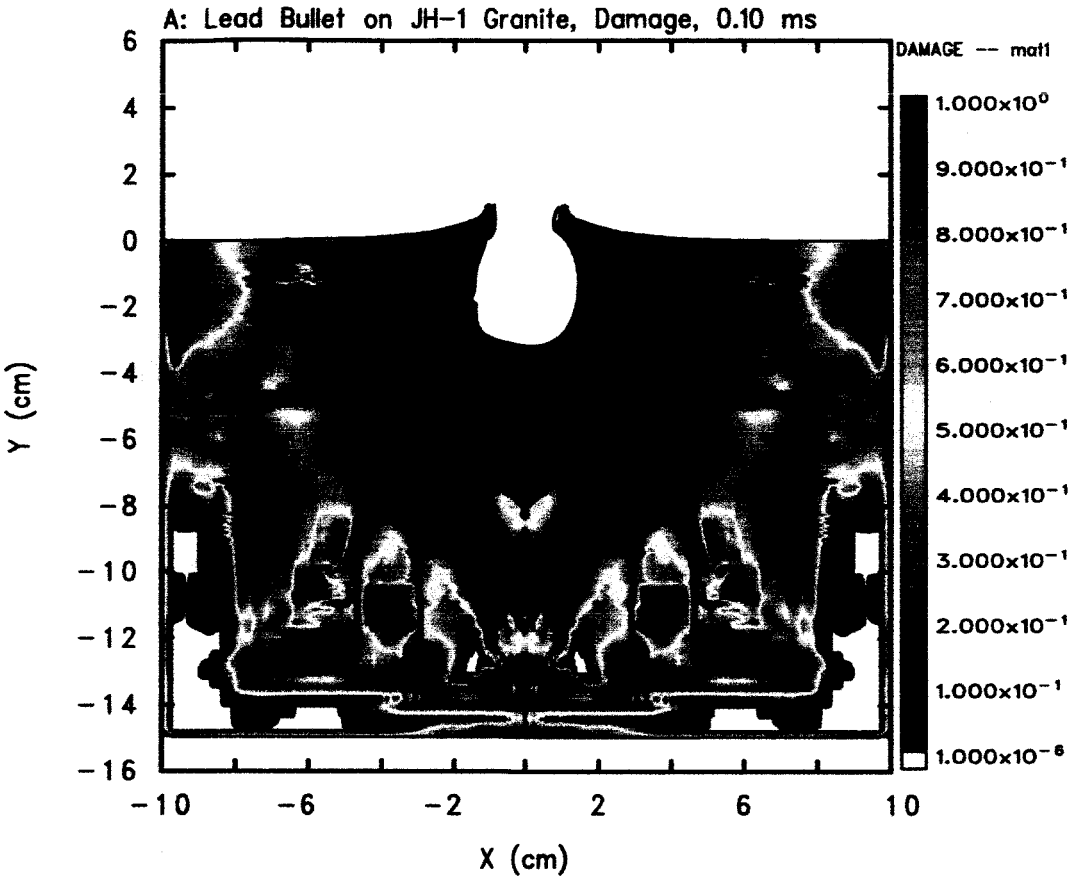

FIGURE 4. 2D simulated damage profile calculated with CTH for shot 117. A lead bullet impacts a granite target, using the JH-1 model at t=0.10 ms. The black line outlines the measured low compressional velocity damaged zone of this shot. Damage is defined by the damage parameter, D. D = 1 (red in the scale) represents fully damaged, and D = 0 (blue in the scale) represents no damage, 0<D<1 means partly damaged. The simulated result overestimates the damage in the granite target produced by the lead impact, indicating that the JH model (Table 2) is not appropriate for predicting damage in granite.

Table 1a: Experimental parameters for San Marcos gabbro (P_c = 150±15 MPa, ρ = 2.867 g/cm^3)

Shot No.	Projectile					Damage depth (cm)		
	material	ρ (g/cm^3)	mass (g)	vel (km/s)	θ	Dicing	Tomography	Predicted
rifle_116	Al2024	2.785	0.7455	1.2	90°	/	2.5~3	3±0.2

Table 1b: Experimental parameters for San Marcos granite (P_c = 130±10 MPa, ρ = 2.66 g/cm^3)

Shot No.	Projectile					Damage depth (cm)		
	material	ρ (g/cm^3)	mass (g)	vel (km/s)	θ	Dicing	Tomography	Predicted
rifle_117	Pb	11.35	3.2	1.18	90°	6	7±1	6~6.5
rifle_120	Pb	11.35	2.92	1.03	90°	/	4±1	4±0.2
rifle_121	Pb	11.35	3.2	1.196	45°	/	3~3.5	?
20mm_1177	Al2024	2.785	1.26	1.2	90°	/	8±1	5~5.5*

Table 1c: Experimental parameters for Bedford limestone (P_c = 35~60 MPa, ρ = 2.42 g/cm^3)

Shot No.	Projectile					Damage depth (cm)		
	material	ρ (g/cm^3)	mass (g)	vel (km/s)	θ	Dicing	Tomography	Predicted
rifle_118	Pb	11.35	3.2	1.162	90°	/	no data	5.5~6
rifle_122	Pb	11.35	3.2	1.159	45°	/	no data	?

/ measuring in process.
* sabot not considered in the prediction; might cause great error.
? Theory needed for oblique impact case to predict damage depth.

Tabel 2: granite constants for the JH-1 constitutive model.

Density	$\rho_0 = 2657$ kg/m^3
Elastic constants	
Bulk modulus	$K_1 = 65.8$ GPa
Shear modulus	$G = 30$ GPa
Poisson's ratio	$\upsilon = 0.29$
Strength constants	
Hugoniot elastic limit	HEL = 4.5 GPa
HEL strength	$\sigma_{HEL} = 2.655$ GPa
HEL pressure	$P_{HEL} = 2.727$ GPa
HEL volumetric strain	$\mu_{HEL} = 0.045$
Tensile strength	$T = 0.12$ GPa
Intact strength coefficient	$S_1 = 1.16$ GPa
Intact strength coefficient	$P_1 = 1$ GPa
Intact strength coefficient	$S_2 = 4.5$ GPa
Intact strength coefficient	$P_1 = 1$ GPa
Strain rate coefficient	$C = 0.005$
Failed strength coefficient	$S^f_{\max} = 0.5$ GPa
Failed strength coefficient	$\alpha = 0.20$
Pressure constants	
Bulk modulus	$K_1 = 65.8$ GPa
Pressure coefficient	$K_2 = -23$ GPa
Pressure coefficient	$K_2 = 2980$ GPa
Bulking factor	$\beta = 1.0$
Damge constants	
Damage coefficient	$\varepsilon^f_{\max} = 1$
Damage coefficient	$P_3 = 50$ GPa
Specific heat	$C_v = 0.29$ J/(g*K)

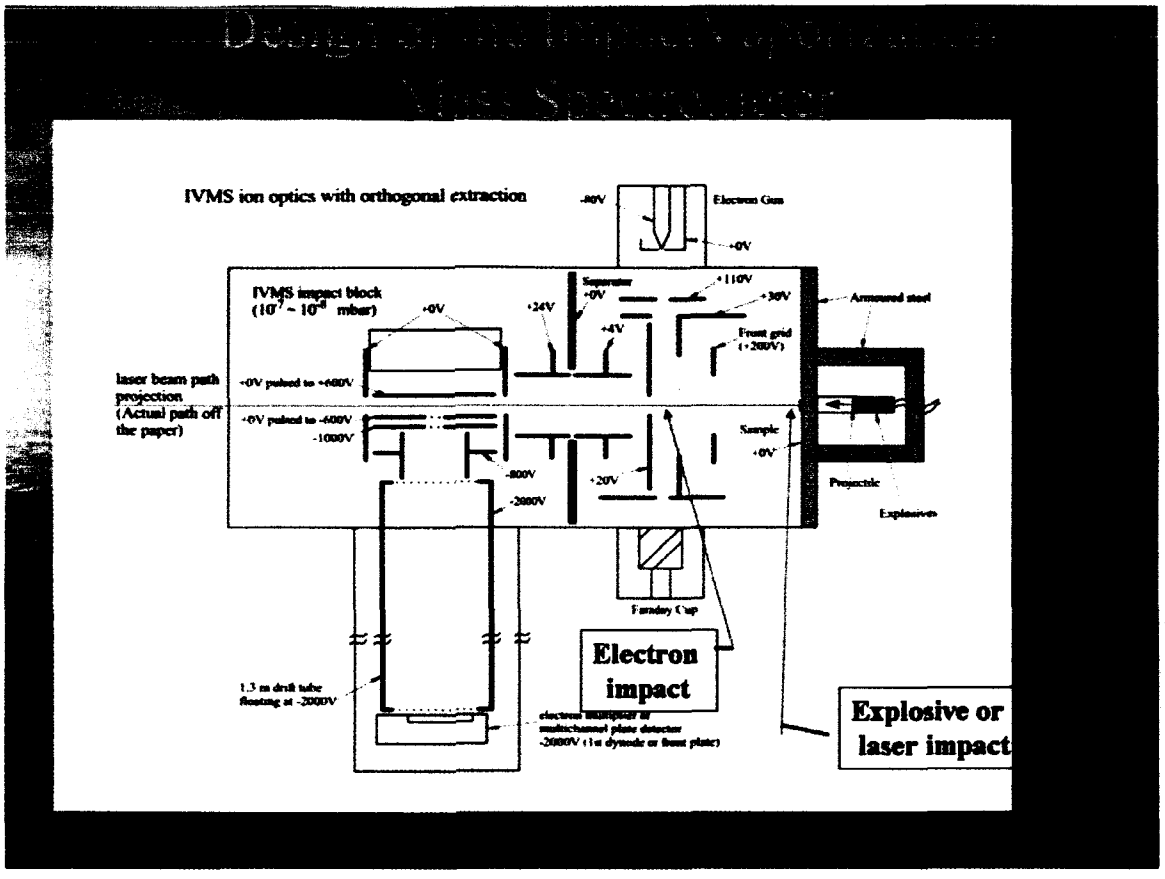

FIGURE 5. Layout of Impact Vaporization Mass Spectrometer (IVMS). This apparatus was built and initially operated during the last year. Initial data were obtained using a laser shock source. Presently, we are developing an explosively launched flyer plate source. Initial data for calcite and gypsum are shown in Figs. 6 and 7. After sample is partially vaporized (right) by explosive source, the electron gun can be used to ionize neutrals or not ionize neutrals. Positive ions are extracted by partial repelling from the +200, +30, +110, +4, and +24 voltage plates in their path. Orthogonal extraction to accomplish acceleration of positive ions is performed with ±600 volt grids.

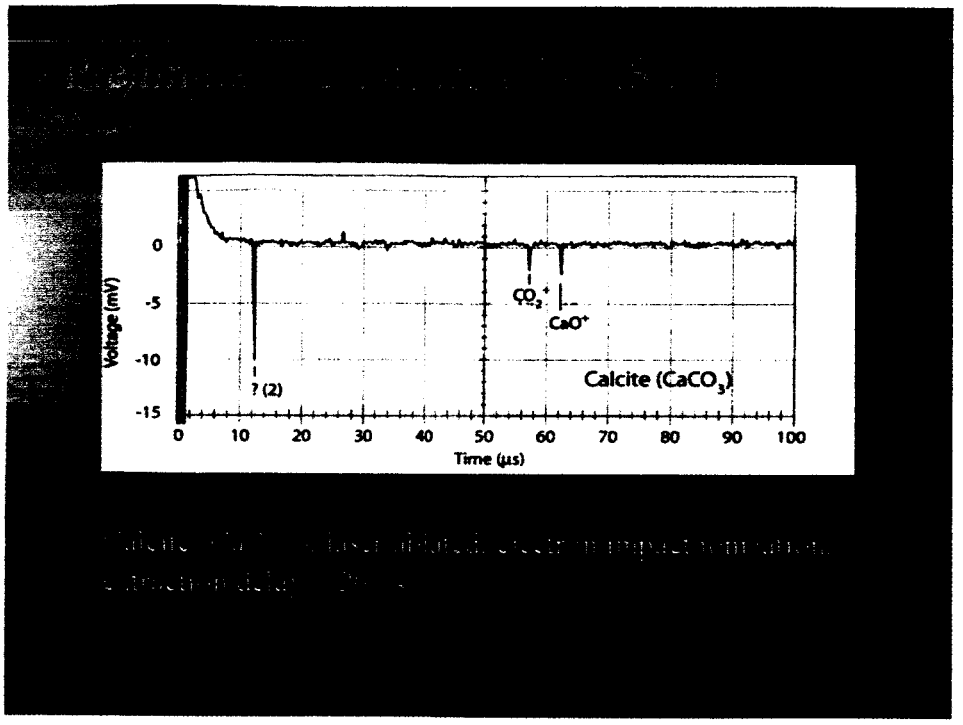

FIGURE 6. Mass spectra from shocked calcite.

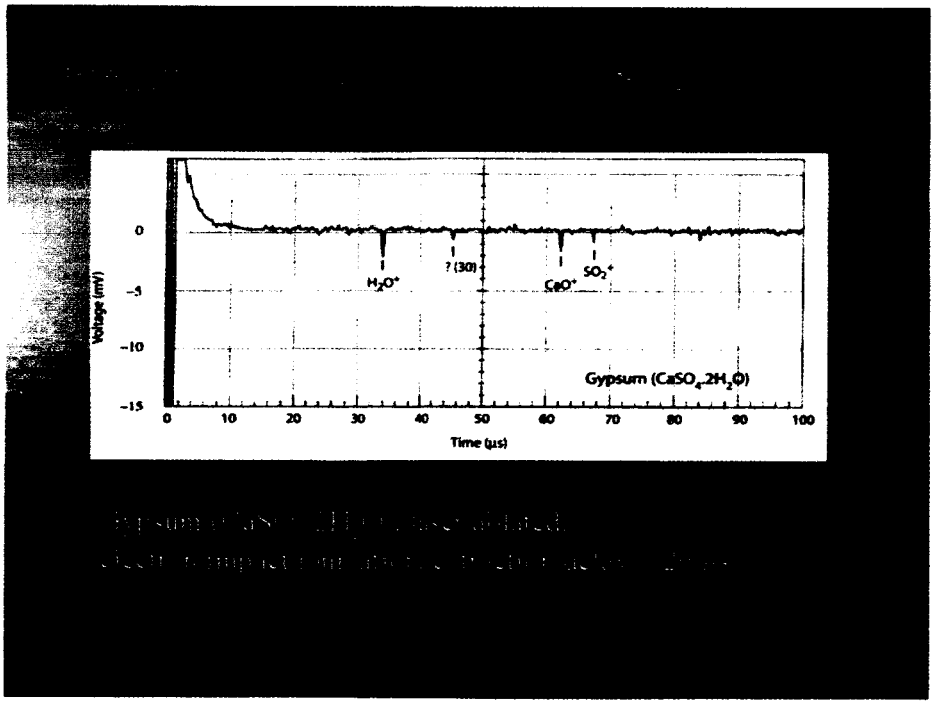

FIGURE 7. Mass spectra from shocked gypsum.

77 °K Planetary ices are plated on Cu target impacted via8*10^7 w/cm^2, 20 ns, 532 nm laser (shock pressures ~vaporization levels)

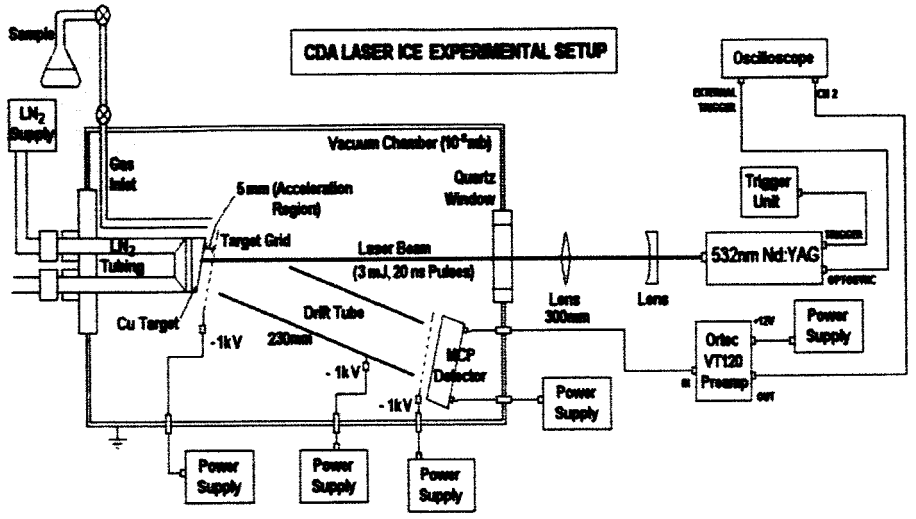

FIGURE 8. IVMS applied to obtain mass spectra for planetary ices. Preliminary results are shown for H_2O and D_2O in Figs. 9 and 10.

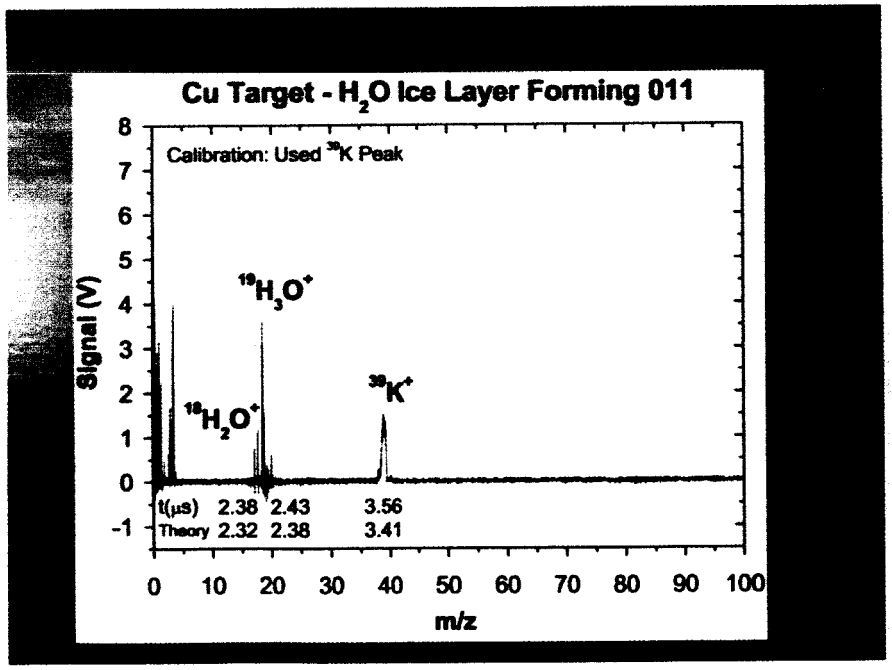

FIGURE 9. $^{18}H_2O^+$ and $^{19}H_3O^+$ ions are seen in the spectra from impacts into water ice.

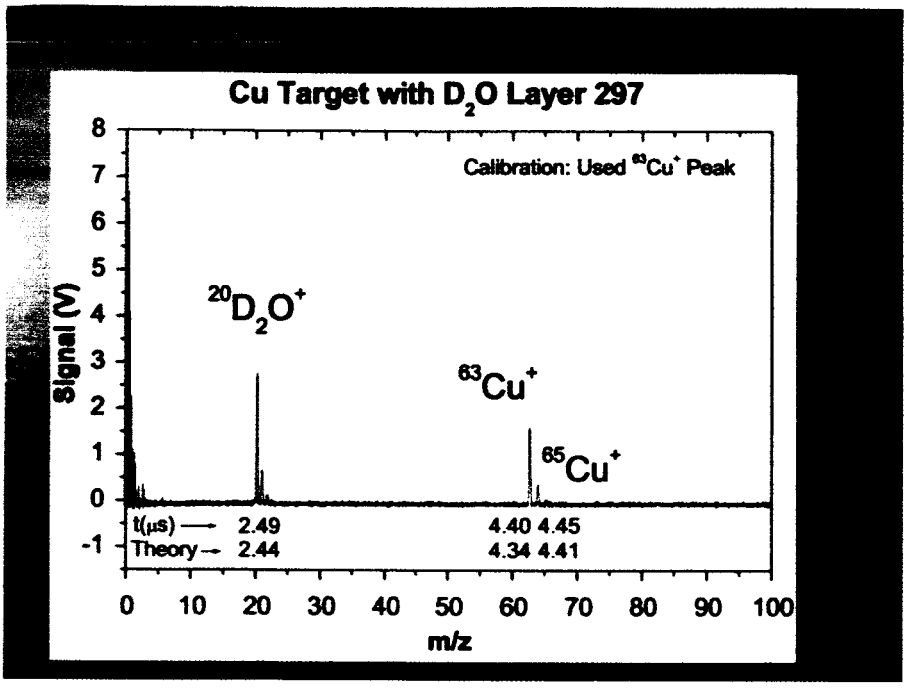

FIGURE 10. Mass spectra for $^{20}D_2O^+$.

References

Ahrens, T.J., S.C. Gupta, G. Jyoti, and J.L. Beauchamp, Mass spectrometer calibration of Cosmic Dust Analyzer, *J. Geophys. Res. - Planets, 108, No. E2, 5007, doi:10.1019/2002JE001912*, 1-1 to 1-10, 2003.

Ahrens, T.J., and J.D. O'Keefe, Shock melting and vaporization of lunar rocks and minerals, *The Moon, 4*, 214-249, 1972.

Ahrens, T.J., and D.K. Potter, Dynamic consolidation of initial diamond single crystal powders and diamond-graphite into fused polycrystalline diamond, in *Shock Waves in Condensed Matter-1987*, edited by S.C. Schmidt, and N.C. Holmes, pp. 419-422, Elsevier Science Publishers B.V., Amsterdam, the Netherlands, 1988.

Ahrens, T.J., and A. Rubin, One- and three-dimensional impact-induced tensional failure in rock, in *Shock Compression of Condensed Matter 1991*, edited by S.C. Schmidt, R.D. Dick, J.W. Forbes, and D.G. Tasker, pp. 579-582, Elsevier Science Publishers B.V., 1992.

Ahrens, T.J., and A.M. Rubin, Impact-induced tensional failure in rock, *J. Geophys. Res., 98*, 1185-1203, 1993.

Ai, H.-A., and T.J. Ahrens, Dynamic tensile strength of terrestrial rocks and application to impact cratering, *Meteorit. Planet. Sci. - Special Issue, 39*, 233-246, 2004.

Ashby, M.F., and C.G. Sammis, The damage mechanics of brittle solids in compression, *Pure Appl. Geophys., 133*, 489-521, 1990.

Boslough, M.B., R.J. Weldon, and T.J. Ahrens, Impact-induced water loss from serpentine, nontronite, and kernite, in *Proc. Lunar Sci. Conf.*, pp. 2145-2158, Pergamon Press, Houston, TX, 1980.

Budiansky, B., and R.J. O'Connell, Elastic moduli of a cracked solids, *Int. Journal Solids Structures, 12*, 81-97, 1976.

Clegg, R.A., C.J. Hayhurst, and I. Robertson, Development and application of a Rankine plasticity model for improved prediction of tensile cracking in ceramic and concrete materials under impact, in *14th DYMAT Technical meeting, November 14-15, 2002*, Sevilla, Spain, 2002.

Collins, G.S., H.J. Melosh, and B.A. Ivanov, Modeling damage and deformation in impact simulations, *Meteor. Planet. Sci., 39* (2), 217-231, 2004.

Holmquist, T.J., G.R. Johnson, and W.H. Cook, A computational constitutive model for concrete subjected to large strains, high strain rates and high pressures, in *14th International Symposium on Ballistics*, Quebec City, Canada, 1993.

Johnson, G.R., and T.J. Holmquist, An improved computational model for brittle materials, in *High-Pressure Science and Technology-1993*, edited by S.C. Schmidt, J.W. Shaner, G.A. Samara, and M. Ross, pp. 981-984, AIP Press, Woodbury, NY, 1994.

Jyoti, G., S.C. Gupta, T.J. Ahrens, D. Kossakovski, and J.L. Beauchamp, Mass spectrometer calibration of high velocity impact ionization based cosmic dust analyzer, *Intl. J. Impact Engng., 23*, 401-408, 1999.

Lange, M.A., and T.J. Ahrens, The evolution of an impact-generated atmosphere, *Icarus, 51*, 96-120, 1982.

Liu, C., and T.J. Ahrens, Stress wave attenuation in shock-damaged rock, *J. Geophys. Res., 102* (B3), 5243-5250, 1997.

Pierazzo, E., and H.J. Melosh, Understanding oblique impacts from experiments, observations and modeling, *Ann. Rev. Earth Planet. Sci*, *28*, 141-167, 2000.

Polanskey, C., and T.J. Ahrens, Impact spallation experiments: Fracture patterns and spall velocities, *Icarus*, *87*, 140-155, 1990.

Pope, K.O., K.H. Baines, A.C. Ocampo, and B.A. Ivanov, Energy, volatile production, and climatic effects of the Chicxulub Cretaceous/Tertiary impact, *J. Geophys. Res.*, *102 (E9)*, 21645-21664, 1997.

Potter, D.K., and T.J. Ahrens, Dynamic consolidation of diamond powder into polycrystalline diamond, *Appl. Phys. Lett.*, *51*, 317-319, 1987.

Potter, D.K., and T.J. Ahrens, Shock-induced formation of $MgAl_2O_4$ spinel from oxides, *Geophys. Res. Lett.*, *21*, 721-724, 1994.

Schwarz, R.B., P. Kasiraj, T. Vreeland, Jr., and T.J. Ahrens, The effect of shock duration on the dynamic consolidation of powders, Chapter X:2, in *Shock Waves in Condensed Matter- 1983*, edited by J.R. Asay, T.A. Graham, and G.K. Straub, pp. 435-438, Elsevier Science Publishers B.V., 1984a.

Schwarz, R.B., P. Kasiraj, T. Vreeland, Jr., and T.J. Ahrens, A theory for the shock-wave consolidation of powders, *Acta Metall.*, *32*, 1243-1252, 1984b.

Sugi, N., M. Arakawa, A. Kouchi, and N. Maeno, In-situ mass spectrometric observation of impact vaporization of water-ice at low temperatures, *Geophys. Res. Lett.*, *25*, 837-840, 1998.

Tyburczy, J.A., R.V. Krishnamurthy, S. Epstein, and T.J. Ahrens, Impact-induced devolatilization and hydrogen isotopic fractionation of serpentine: Implications for planetary accretion, *Earth Planet. Sci. Lett.*, *98*, 245-261, 1990.